# Binding and discerning interactions of PTP1B allosteric inhibitors: Novel insights from molecular dynamics simulations

Ranajit Nivrutti Shinde, M. Elizabeth Sobhia *

*Department of Pharmacoinformatics, National Institute of Pharmaceutical Education and Research (NIPER), S.A.S. Nagar, Punjab 160062, India*

## ABSTRACT

The $\alpha 7$ helix is either disordered or missing in the three co-crystal structures of allosteric inhibitors with protein tyrosine phosphatase 1B (PTP1B). It was modeled in each complex using the open form of PTP1B structure and studied using molecular dynamics (MD) simulations for 25 ns. *B*-factor analysis of the residues sheds light on its disordered nature in the co-crystal structures. Further, the ability of inhibitors to act as allosteric inhibitor was studied and established using novel hydrogen bond criteria. The MD simulations were utilized to determine the relative importance of electrostatic and hydrophobic component in to the binding of inhibitors. It was revealed that the hydrophobic interactions predominantly drive the molecular recognition of these inhibitors. Per residue energy decomposition analysis attributed dissimilar affinities of three inhibitors to the several hydrogen bonds and non-bonded interactions. Among the secondary structure elements that surround the allosteric site, helices $\alpha 6$, $\alpha 7$ and loop $\alpha 6$–$\alpha 7$ were notorious in providing variable affinities to the inhibitors. A novel hydrophobic pocket lined by the $\alpha 7$ helix residues Val287, Asn289 and Trp291 was identified in the allosteric site. This study provides useful insights for the rational design of high affinity PTP1B allosteric inhibitors.

© 2013 Elsevier Inc. All rights reserved.

## 1. Introduction

Druggable targets that can ameliorate insulin resistance and associated complications are increasingly gaining importance. Protein-tyrosine phosphatase 1B (PTP1B) has been widely acknowledged as a key negative regulator of tyrosine phosphorylation associated with insulin receptor signaling [1]. Mice lacking this enzyme are protected from diet-induced obesity [2] and effects on PTP1B knockout mice are also shown to be insulin action specific [3]. Such studies have proposed PTP1B inhibitors as "potential insulin sensitizers" in the management of type 2 diabetes [4].

PTP1B is one of the most widely studied phosphatase for which 121 structures and 133 chains are available in protein databank (PDB) [5]. 3D structure of PTP1B is shown in Fig. 1. It has evolved with the positively charged active site to accommodate two negative charges of phosphotyrosine. This has made large molecules and multiple charges as essential prerequisites for ligands to act as potential competitive inhibitors. Owing to this, active site directed molecules are not drug-like and have shown limited cell membrane permeability [6]. A good selectivity is another essential feature required for the development of PTP1B inhibitors. Alignment of 37 human PTP domains has shown conservation of the WPD-loop

(Trp179, Pro180 and Asp181) with greater than 80% identity [7]. In addition, active site residues, 214–221, were also found to have 100% identity except Ala217 and Ile219 which showed 90% and 40% identity respectively. These residues are involved in the binding and catalysis of the substrate. As all members of protein tyrosine phosphatase family share such a high degree of structural conservation in the phosphotyrosine binding pocket, designing selective inhibitors for PTP1B poses a great challenge. TCPTP, the closest structural homologue of PTP1B displays 65% sequence identity overall and 72% identity within the conserved catalytic domain with PTP1B [8]. Additionally, TCPTP knockout mice have shown defects in bone marrow, B cell lymphopoiesis, and erythropoiesis, as well as impaired T and B cell functions. Thus, it makes indispensable for every inhibitor of PTP1B to have a good selectivity [9].

Recently, crystallographic study has revealed another binding site located at a distance of ~20 Å from the catalytic site (Fig. 1) [10]. Inhibitor binds to this site and attenuates PTP1B by the allosteric mechanism. Such types of three inhibitors have been identified, and their co-crystal structures are available in the PDB (Table 1). Mechanistically, an allosteric inhibitor locks PTP1B in the 'open' conformations and prevents its conversion into the 'close' conformation, which is essential for substrate catalysis (Fig. 2) [10].

In the open conformation (apo form), the WPD-loop is moved back and the catalytic pocket becomes accessible to the substrate. Whereas, in the closed conformation, WPD-loop bends over the

---

* Corresponding author. Tel.: +91 172 2214682x687 fax: +91 172 2214692.
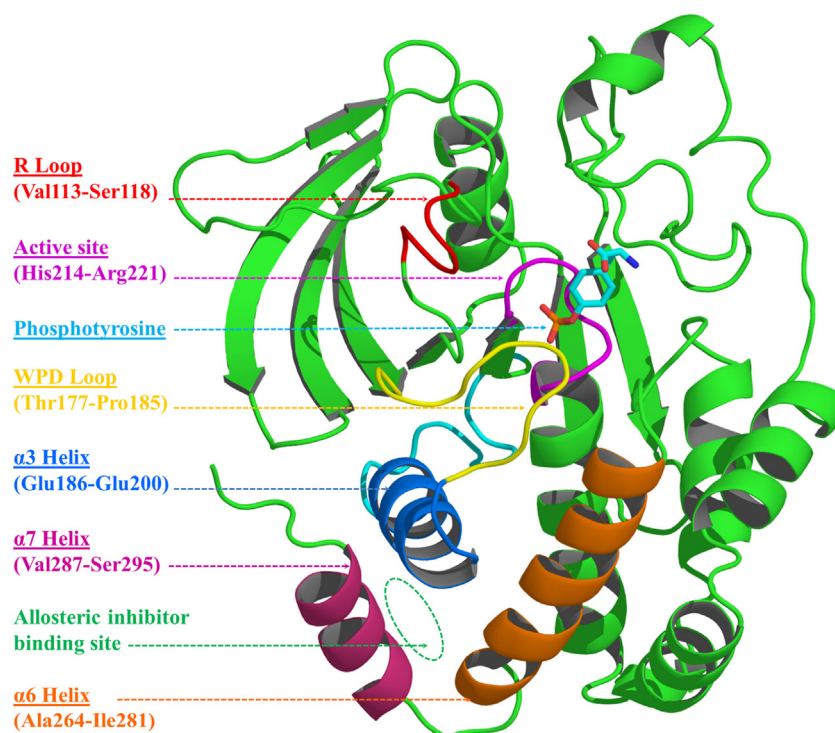 *E-mail address:* mesophia@niper.ac.in (M.E. Sobhia).

**Fig. 1.** Phosphotyrosine bound structure of PTP1B (PDB ID: 1PTV), with important regions highlighted. An allosteric inhibitor binds to a site surrounded by the three helices, α3, α6 and α7.

phosphotyrosine, traps it and positions Asp181 in such a way that it would carry out acid and base catalysis (Fig. 2) [11]. The closing of the WPD-loop, in part, is a result of an extensive series of hydrogen bond (H-bond) interactions between α7–α3–α6 helices. The allosteric inhibitor blocks these interactions by placing itself between these helices. Among three helices, interactions with α7 helix are essential as the inhibitor creates space for its binding by displacing Trp291 of the α7 helix from its position. Truncation of



**Fig. 2.** Overlay of three PTP1B structures, with depiction of α3 helix and WPD loop; cyan, 1PTY, 'close' conformation bound to phosphotyrosine; magenta, 2HNP, apo enzyme in 'open' conformation; green, 1T48, allosteric inhibitor bound PTP1B. Allosteric inhibitor stabilizes open conformation, forbidding closure of WPD loop.

this helix has shown a four-fold decrease in the catalytic activity of PTP1B, confirming its significance [12].

Molecular dynamics (MD) studies have been performed on the PTP1B having modeled α7 helix [13–17]. MD is an effective approach to analyze the time dependent behavior of various interactions and conformational changes. Modified MD protocols, e.g. steered, targeted, coarse-grained, etc., are being used to reduce the time period of total simulation and study the course of several processes such as ligand binding/unbinding, ion transfer, loop movement, and protein folding. Kamerlin el al. have reported two such studies, where they performed MD and targeted-MD simulations to understand the structural changes associated with the closing of WPD-loop in the presence and absence of Inhibitor-1 [13,14]. It was observed that the movement of the WPD-loop from the 'open' state to the 'closed' state occurs due to several interactions formed within the residues of different secondary structure elements. During the WPD-loop closure, α3 helix was observed to contract by a distance of 2.5 Å. In the presence of the allosteric inhibitor, this helix and S-loop showed reduced flexibility compared to the flexibility in the open and closed WPD-loop structures. Olmez et al. analyzed the conformational changes in the secondary structure elements of PTP1B in the presence and absence of α7 helix [16]. In a novel study that explored interactions between Inhibitor-2 and allosteric site, Bharatham et al. used MD generated protein flexibility to develop receptor based pharmacophore models for the Inhibitor-2 (Table 1) [15]. The three pharmacophore models contained six features; H-bond donor (sulfonamide amino group), H-bond acceptor (carbonyl group), three ring-aromatics (benzofuran core, dibromo phenol group and phenyl sulfonamide group), and one hydrophobic group (ethyl group) (Table 1). These models were thereafter utilized to screen the databases. Similarly, Lee et al. used molecular docking methodology to demonstrate the interactions of the non-competitive inhibitor amentoflavone, a naturally occurring bioflavonoid, at the allosteric site [18]. These interactions were utilized to develop
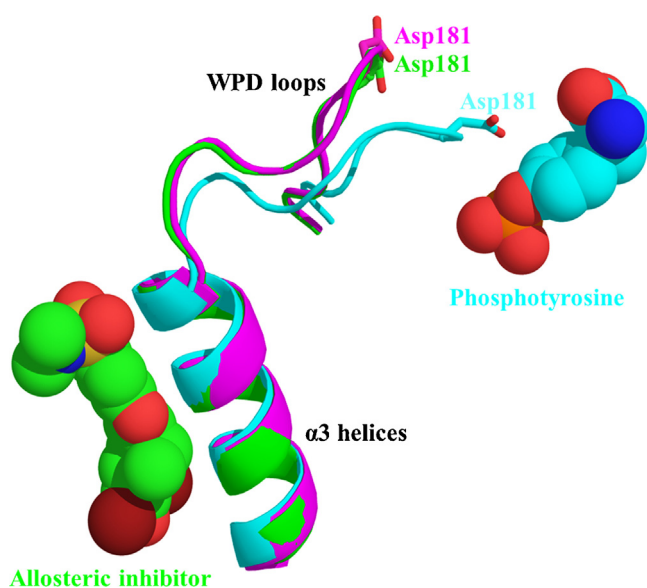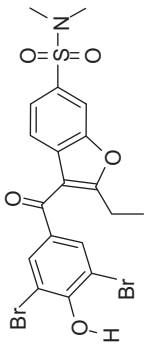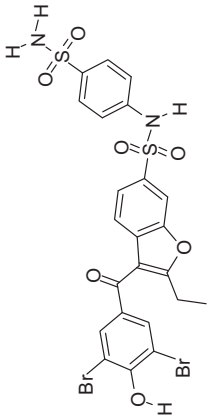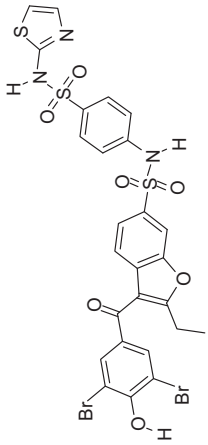
**Table 1**

Structure of allosteric inhibitors with their inhibitory activity against PTP1B. Last row shows the protein data bank entry name for their co-crystal structures.

| Name | Inhibitor-1 | Inhibitor-2 | Inhibitor-3 |
|---|---|---|---|
| Structure | | | |
| $IC_{50}$ (μM) | 350.00 | 22.00 | 8.00 |
| PDB ID | 1T48 | 1T49 | 1T4J |

the receptor oriented pharmacophore model. This study finally proposed sumaflavone and tetrahydroamentoflavone as potential allosteric inhibitors of PTP1B. Recently, Baskaran et al. studied the binding mechanism of non-competitive inhibitors chlorogenic acid and cichoric acid, at the allosteric site. MD simulations performed on these inhibitors showed several stable interactions between the inhibitors and allosteric site residues [17]. Another study monitored interactions of Inhibitor-1 using per residue energy decomposition analysis and demonstrated the importance of VDW interactions in the binding and stability of the WPD loop [19].

Till date, studies have been directed either to understand the molecular changes associated with the allosteric inhibition, the pharmacophore features associated with the inhibitors [13–15] or the interactions of the single inhibitor [19]. Nevertheless, these studies also have shed light on the interactions of the Inhibitor-1 and Inhibitor-2 at the allosteric site. However, the complete interaction and energetic profile of these inhibitors at the allosteric site is still unexplored. Molecular forces that govern the differential affinity and activity of these inhibitors are not studied. In this regard, our group has earlier reported preliminary results of the Inhibitor-3 binding interactions [20]. We have also revealed five novel H-bonds which can be utilized as the geometric criteria for the characterization of conformational states of WPD-loop and the allosteric inhibition potential of new inhibitors [21]. The present work is an extension of these studies to the allosteric Inhibitors-1, 2 and 3 (Table 1) and explores the complete interaction and energy profile of these inhibitors using Molecular mechanics-Poisson-Boltzmann surface area and -generalized Born surface area (MM-PBSA/GBSA) methods. The results were comparatively analyzed to understand the interactions essential for the binding and affinity of the three inhibitors.

## 2. Materials and methods

### 2.1. Modeling of α7 helix of PTP1B

The crystal structure of PTP1B in apo form shows α7 helix and loop connected to it [22]. Residues corresponding to this part span from 282 to 298. 282–286 define the α6-α7 loop, 287–295 defines the α7 helix while, 296–298 are the terminal residues. PTP1B co-crystal structures 1T48, 1T49 and 1T4J have revealed the binding of allosteric inhibitors in this region [10]. However, in the presence of Inhibitors-1, 2 and 3 (Table 1), these residues are either disordered (PDB ID: 1T48) or not modeled (PDB ID: 1T49 and 1T4J). The allosteric site is adaptive binding site and formed only in the presence of the allosteric inhibitor. The inhibitor dislodges Trp291 from its position and accommodates its benzofuran ring at the place of the indole ring. Subsequently, the side chains of Phe192, Phe280 and Glu276 make movements to favor the binding. Being adaptive in nature, the allosteric site can take different conformations to accommodate the incoming ligand. Hence, we decided to model the residues 282–298 to the individual co-crystal structures of Inhibitors-1, 2 and 3 (1T48, 1T49, and 1T4J respectively). Human PTP1B structure 2f6f, which exists in the open conformation, was selected to model these residues as the co-crystal structures are also present in the open conformation [12]. Residues were modeled around the bioactive conformation of inhibitors using Modeler9v8 program [23]. H-bond interactions made by the carbonyl oxygen of the inhibitors with the side chain nitrogen of Asn193 and phenyl sulfonamide nitrogen of the inhibitor with the side chain carboxyl oxygen of Glu276 as observed in the co-crystal structures were considered as essential requirement for the selection of models. α7 helix modeled complexes of Inhibitors-1, 2 and 3 were then subjected to the MD studies [10].

## 2.2. System preparation for the MD simulations

MD simulations were performed on each of the three PTP1B-inhibitor complex systems. AM1-BCC method was used to assign partial atomic charges of inhibitors [24,25], while general amber force field (GAFF) was used to create the topology [26]. Protein topology was prepared with FF99SB force field. Further, the protein-inhibitor complexes were processed by xLeap module where individual complex was solvated with TIP3P water model by creating an isometric water box, where the edge of the water box was 9.0 Å from the periphery of protein [27]. The systems were neutralized by adding counter ions (Na$^+$). Thus prepared systems were saved in topology and coordinate files and were used as input to perform the MD using SANDER module of AMBER [28]. Initially, heating was performed with NVT ensemble by keeping the protein–ligand complex restrained with force constant of 2 kcal/mol/Å$^2$. Density equilibration was then performed with the same restrain force on the complex. The system was further equilibrated under constant pressure at 300 K for the period of 5 ns. The final production simulation was performed for 20 ns on NPT ensemble at 310 K and 1 atm. The step size of 2 fs was kept throughout the simulation. Langevin thermostat and barostat were used for temperature and pressure coupling. SHAKE algorithm was applied to constrain all the bonds containing hydrogen atoms [29]. Non-bonded cutoff was kept at 8 Å and long range VDW interactions were treated by Particle Mesh Ewald method (PME) with fast Fourier transform grid spacing of approximately 0.1 nm [30]. Trajectory snapshots were taken at an interval of 2 ps and used for the final analysis.

## 2.3. Free energy calculations

The binding affinity of inhibitors can be studied using binding free energy. It was estimated using the MM-PBSA and MM-GBSA methods [31,32]. Additionally, different components of the interaction energy that contribute to the binding were estimated. They include van der Waals (VDW), electrostatic, polar solvation, and nonpolar solvation interaction energy. Here the entropy was not calculated, as the inhibitors are very similar (analogs) to each other. Binding free energy ($\Delta G_{Bind}$) of inhibitor at the allosteric binding site on PTP1B was calculated as follows:

$$\Delta G_{Bind} = G_{Complex} - G_{Protein} - G_{Ligand} \tag{1}$$

where, $G_{Complex}$, $G_{Protein}$ and $G_{Ligand}$ are the free energies of complex, protein (PTP1B), and ligand (inhibitor), respectively. Free energy ($G$) of each state was calculated as follows:

$$G = E_{MM} + G_{PB/GB} + G_{SA} - TS \tag{2}$$

$$E_{MM} = E_{vdw} + E_{ele} + E_{int} \tag{3}$$

where $E_{MM}$ is the molecular mechanical energy, $G_{PB/GB}$ is polar contribution toward solvation energy calculated either by Poisson-Boltzmann (PB) or generalized Born (GB) method respectively. $G_{SA}$ is the contributions from nonpolar terms toward solvation energy, and TS is the entropic contribution of the inhibitor. $E_{MM}$ was obtained by summing the contributions from electrostatic energy ($E_{ele}$), VDW energy ($E_{vdw}$), and internal energy including bond, angle and torsional angle energy ($E_{int}$) using the same force field as that of MD simulations. $G_{PB}$ was calculated using the DELPHI program [33] while $G_{GB}$ was calculated with Onufriev's method [34]. $G_{SA}$ in Eq. (2) is proportional to the solvent accessible surface area (SASA) and was computed by molsurf module using the Eq. (4)

$$G_{SA} = \gamma * SASA + b \tag{4}$$

In Eq. (4), the surface tension proportionality constant ($\gamma$) was set to 0.0072 kcal/mol/Å$^2$, while the free energy of nonpolar

solvation for a point solute (b) was set to a default value of 0 kcal/mol. SASA was computed by molsurf using a fast algorithm called the Linear Combinations of Pairwise Overlaps (LCPO), which simply computes a surface area of two overlapping atoms by subtracting their overlapping region from the total area of their VDW surfaces. VDW radii in AMBER and GAFF force fields were used to define solute atoms which were then augmented by a probe sphere of 1.4 Å for the molsurf computations. Binding free energy calculations were averaged over 500 frames taken at the interval of 40 ps over the production run of 20 ns.

## 2.4. B-factor analysis

Crystal structure analyses of several PTP1B inhibitor complexes revealed that PTP1B undergoes conformational changes in helices and loops. To compare the flexibility of the structures, the isotropic temperature factor ($B$) was calculated. The $B$ factor was used to calculate the mobility of the residues present in the α7 helix. It was calculated from mean square fluctuations (msf) using the following equation:

$$B = \left[ \frac{8\pi ** 2}{3} \right] (msf) \tag{5}$$

The $B$ factor was calculated using the equation for each residue and plotted against each residue.

## 2.5. Energy decomposition analysis

Free energy was decomposed to estimate the contribution of each residue in the inhibitor binding process, and was performed by using MM-GBSA method [35]. Energy of each residue–inhibitor interaction is given by following equation:

$$\Delta G_{residue-inhibitor} = \Delta E_{ele} + \Delta E_{vdW} + \Delta G_{GB} + \Delta G_{SA} \tag{6}$$

where, $\Delta G_{GB}$ is the polar group contribution to the solvation free energy calculated using generalized Born model. $\Delta G_{SA}$ is the nonpolar group contribution to the solvation free energy calculated using ICOSA method. Similar to the binding free energy, the decomposition energy was also averaged over 20 ns of the production run.

# 3. Results and discussion

## 3.1. RMSD analysis

In order to assess the stability of systems during the MD simulations, RMSD values for all backbone atoms was calculated by aligning all MD generated conformations to the initial structure. RMSD plot for the complexes during a course of MD production simulation is shown in Fig. 3. It shows that the complexes of Inhibitors 1, 2 and 3 are stable during the production phase of 20 ns. For Inhibitor-1 complex, the RMSD ranged between 1.43 Å and 2.10 Å with an average value of 1.73 Å. The Inhibitor-2 complex showed the RMSD of 1.46–2.31 Å with an average value of 1.90 Å while Inhibitor-3 complex had the RMSD of 1.40–2.24 Å with 1.77 Å as the average value. During simulation, many other parameters such as pressure, molecular density, temperature and other energy components were monitored to ensure that the systems were stable. The analysis revealed that the trajectories were stable enough and could be used for free energy calculations.

## 3.2. Geometric analysis

As discussed earlier, WPD-loop in the PTP1B exists in an open and closed conformation. Closure of WPD-loop is essential for the
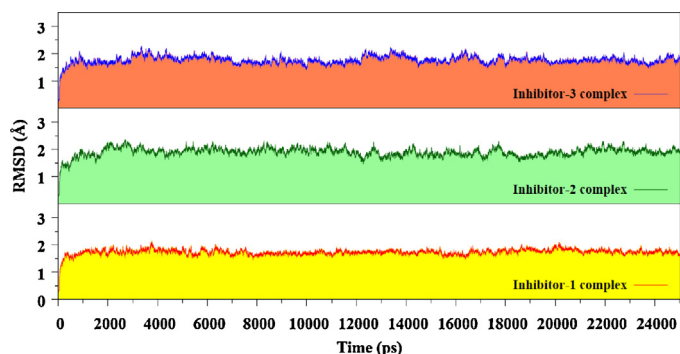
**Fig. 3.** Plot of the RMSD with respect to time for the complexes of PTP1B with Inhibitor-1, Inhibitor-2 and Inhibitor-3 shown in red, green and blue line respectively. (For interpretation of the references to color in this figure legend, the reader is referred to the web version of this article.)

efficient dephosphorylation of substrate. Allosteric inhibitor stabilizes the WPD-loop in the open conformation and precludes the changes that are necessary for the closure of the WPD-loop. Kamerlin et al. identified these changes and used them as geometrical criteria to characterize the conformation of the WPD-loop as either open or closed [14]. In our recent study, we updated these criteria considering additional PTP1B structures and established five additional criteria [21]. They were used to assess the states (open/close) of WPD-loop during simulations. Inhibitors used in our study are known allosteric inhibitors and are expected to keep the WPD-loop in open conformation. It was observed that all the three systems followed the geometrical criteria of the open conformation (Supplementary information, Table S1). This confirmed that the inhibitors stabilized WPD-loop in the open conformation during the simulation period which is in accordance with the mechanism of allosteric PTP1B inhibition [10].

### 3.3. B-factor analysis

Wiesmann et al. [10] have shown that the allosteric inhibitors bind to an adaptable region. During this binding, residue Trp291 of $\alpha 7$ helix is observed to be displaced by the benzofuran core of inhibitors, suggesting a significant movement of the $\alpha 7$ helix in the presence of allosteric inhibitors. Hence, it was interesting to observe the behavior of $\alpha 7$ helix residues in the presence of three inhibitors in our study. B-factors for individual residues (282–295) were calculated for all the three complexes (Fig. 4). It was observed, for the PTP1B-Inhibitor-1 complex, that the residues were comparatively more stable with an average B-factor of 76.92 $\text{Å}^2$. This was attributed to the small size of the Inhibitor-1 (Table 1), which accommodated into the groove without



**Fig. 4.** B-factor plot for the residues 287–295 in PTP1B-Inhibitor-1, Inhibitor-2 and Inhbiitor-3 complexes.

**Table 2**

Binding free energy and its components for Inhibitors-1, 2 and 3 in kcal/mol. VDW = van der Waals energy calculated by the molecular mechanics (MM). ELE = electrostatic energy calculated by MM. GAS = total gas phase energy (sum of ELE and VDW). PBSUR/GBSUR = nonpolar contribution to the solvation free energy. PBCAL/GBCAL = the electrostatic contribution to the solvation free energy calculated by PB or GB respectively. PBSOL/GBSOL = sum of nonpolar and polar contributions to solvation. PBTOT/GBTOT = final estimated binding free energy calculated from the terms above.

| | Inhibitor-1 | | Inhibitor-2 | | Inhibitor-3 | |
|---|---|---|---|---|---|---|
| VDW | −53.68 | 2.90 | −66.45 | 3.16 | −74.94 | 3.82 |
| ELE | −15.40 | 4.08 | −37.33 | 6.08 | −50.70 | 6.95 |
| GAS | −69.09 | 4.76 | −103.78 | 6.00 | −125.64 | 7.10 |
| | | | | | | |
| PBSUR | −3.92 | 0.11 | −4.67 | 0.09 | −5.35 | 0.12 |
| PBCAL | 39.89 | 4.31 | 55.69 | 4.67 | 67.28 | 5.78 |
| PBSOL | 35.97 | 4.28 | 51.02 | 4.65 | 61.93 | 5.75 |
| PBTOT | −33.12 | 3.43 | −52.76 | 3.83 | −63.71 | 4.13 |
| | | | | | | |
| GBSUR | −5.79 | 0.26 | −7.08 | 0.16 | −7.94 | 0.21 |
| GBCAL | 25.11 | 4.53 | 50.71 | 4.35 | 58.11 | 5.36 |
| GBSOL | 19.32 | 4.52 | 43.63 | 4.30 | 50.17 | 5.29 |
| GBTOT | −49.77 | 4.08 | −60.15 | 3.69 | −75.47 | 4.65 |

considerable adaptive conformational changes in the $\alpha 7$ helix. In the case of Inhibitor-2 complex, residues 282–295 had B-factors in the range of 49.34–218.85 $\text{Å}^2$, with an average of 134.92 $\text{Å}^2$. Six residues had B-factor above 100 $\text{Å}^2$, which revealed a higher flexibility of PTP1B when bound to the intermediate size inhibitor. In the Inhibitor-3 complex, B-factor ranged from 43.99 $\text{Å}^2$ to 324.57 $\text{Å}^2$, with an average of 152.93 $\text{Å}^2$. Thus, the flexibility of the residues increased with the size of the inhibitor as $\alpha 7$ helix underwent substantial conformational changes to accommodate the incoming Inhibitor. This put forth that the flexibility of residues could be the reason behind the absence of $\alpha 7$ helix in the co-crystal structures of Inhibitors-1, 2 and 3 i.e. 1T48, 1T49 and 1T4J.

### 3.4. Binding free energy

Binding affinity of inhibitors was studied on the basis of binding free energy estimated using MM-PBSA and MM-GBSA methods. The VDW and electrostatic components of energy contributing to the binding of inhibitors were estimated. The entropy was not calculated as we were interested in the comparative analysis of interactions parameters important to the inhibitor binding with PTP1B. This is the first study where an attempt has been made to quantify the interactions between three allosteric inhibitors and the residues of PTP1B. Table 2 provides the details of the binding free energies of the three inhibitors.

Among all the inhibitors, Inhibitor-1 made the least electrostatic interactions (−15.40 kcal/mol) with the PTP1B, while maximum interactions were shown by Inhibitor-3. Inhibitor-2 gained significant VDW contribution over Inhibitor-1 because of the presence of the second sulfonamide group, which showed H-bond interactions with the residues Trp291, Glu276, and Asp284. For Inhibitor-3 additional interactions were observed, as compared to Inhibitor-2, because of the presence of extra thiazole ring, showing $\pi$–$\pi$ stacking interactions. H-bond interactions with Gly283 and Asp284 improved the binding energy of Inhibitor-3 over the other two inhibitors. The contribution of VDW interaction energy increased from Inhibitor-1 to Inhibitor-3 (−53.68 kcal/mol, −66.45 kcal/mol, −74.94 kcal/mol respectively). This increase in the contribution was related to the increase in the number of atoms, which was in turn was related to the increase in the number of rings (two in Inhibitor-1, three in Inhibitor-2, and four in Inhibitor-3). The greater VDW contribution to the Inhibitor-3, over the other inhibitors, was mainly provided by the residues of $\alpha 6$–$\alpha 7$ loop viz. Asp284, Ser285 and Ser286. Thus, both electrostatic and VDW
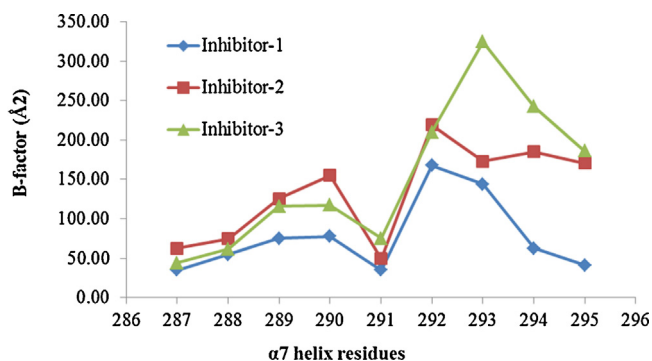
interactions play a critical role in the binding, suggesting that the allosteric site can accommodate polar and nonpolar groups of inhibitors. It offers an opportunity to design novel inhibitors with better permeability and solubility. Additionally, PBTOT and GBTOT energies also followed the trend of experimental $IC_{50}$ values [Inhibitor-1 ($IC_{50}$ = 350 μM), Inhibitor-2 ($IC_{50}$ = 22 μM) and Inhibitor-3 ($IC_{50}$ = 8 μM)] (Table 2).

### 3.5. Energy decomposition

Crystallographic work of Montalibet et al. [12] had shown that the H-bond network formed by the residues of α3–α6–α7 helices is essential for the proper orientation of WPD-loop in the active site. The allosteric inhibitor was shown to disturb this extensive network of H-bonds by positioning itself between the grooves formed by α3–α6–α7 helices [10,15]. This suggested that the interactions of the residues from these helices with the inhibitor play an important role in the binding and stabilization of the complex. Qualification and quantification of these interactions for each residue can provide information about the nature of the binding forces and vital residues that drive the binding of inhibitors at the allosteric site, which consequently can be used for the rational design of more potent and effective inhibitors. MM-GBSA method was utilized in our study to analyze VDW and electrostatic contributions made by the individual residues of α3, α7, α6 helices and α6–α7 loop to the inhibitor binding. The residues contributing more than −0.50 kcal/mol GBTOT energy have been discussed. Their interactions with the individual inhibitor are shown in Fig. 5. For better understanding, sub-structures were used to explain the interactions between the individual residues and inhibitor as shown in Fig. 6.

#### 3.5.1. α3 helix residues

Targeted MD study of PTP1B by Kamerlin et al. showed that the α3 helix contracts by a distance of 2.5 Å during the movement of the WPD-loop from the 'open' to the 'closed' conformation [14]. Allosteric Inhibitor-1 reduced this contraction by making consistent interactions with the Leu192, Asn193, and Phe196 of the α3 helix. Additionally crystallographic studies revealed Leu192 and Phe196 as a part of hydrophobic pocket that accommodates the benzofuran ring of Inhibitor-2 [10]. It concluded that α3 helix residues play a vital role in the stabilization of inhibitors at the allosteric site, closure of WPD-loop and consequently, in the inhibition of PTP1B. We performed per residue energy contribution analysis of α3 helix residues to get the details of their interactions with the three inhibitors.

Our previous work on conformational distinctiveness of PTP1B structures revealed two H-bonds between the residues of α3 helix (geometrical criteria 6 and 7) in the closed state of PTP1B [21]. First H-bond was formed between the backbone oxygen atom of Ser187 and the backbone nitrogen atom of Phe191. Second H-bond was formed between the γ oxygen atom of Ser187 and backbone nitrogen atom of Ser190. Steric clash between Phe269 and Pro188 was shown to be one of the reasons for the reorientation of WPD-loop and formation of these two bonds (Supplementary information, Fig. S1). Interactions of the inhibitor with Pro188 can essentially decrease the steric clash between two residues and in turn avoid the formation of bonds and henceforth, reorientation of the WPD-loop is necessary for catalysis. Decomposition analysis showed that Pro188 offers favorable hydrophobic interactions energy toward the binding of all the three inhibitors (Table 3, and Supplementary information, Fig. S2). Interactions were observed between Pro188 ring atoms and sulfonyl atoms of benzofuran sulfonamide group of inhibitors (Fig. 5). They showed an increasing energy contribution (GBTOT), albeit in small quantity, for Inhibitors 1–3 (−0.55 kcal/mol, −0.67 kcal/mol, −0.79 kcal/mol respectively).

**Table 3**
Binding energy between residues of α3 helix and allosteric inhibitors in kcal/mol.

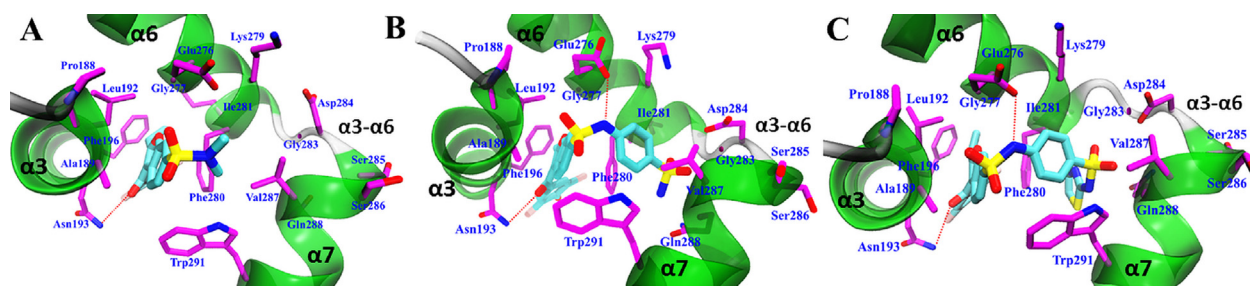| Residue | Inhibitor-1 | | | | | Inhibitor-2 | | | | | Inhibitor-3 | | | | |
|---|---|---|---|---|---|---|---|---|---|---|---|---|---|---|---|
| | Pro188 | Ala189 | Leu192 | Asn193 | Phe196 | Pro188 | Ala189 | Leu192 | Asn193 | Phe196 | Pro188 | Ala189 | Leu192 | Asn193 | Phe196 |
| VDW | −0.39 | −1.32 | −2.34 | −1.30 | −3.20 | −0.56 | −1.76 | −2.82 | −1.64 | −3.33 | −0.65 | −1.81 | −2.83 | −1.57 | −3.37 |
| GBSUR | −0.02 | −0.17 | −0.19 | −0.13 | −0.41 | −0.01 | −0.20 | −0.14 | −0.21 | −0.41 | −0.01 | −0.19 | −0.14 | −0.22 | −0.33 |
| GBVDW | −0.41 | −1.49 | −2.53 | −1.43 | −3.61 | −0.57 | −1.96 | −2.96 | −1.85 | −3.74 | −0.66 | −2.00 | −2.97 | −1.79 | −3.70 |
| ELE | −0.45 | −0.27 | −0.92 | −3.25 | −0.39 | −0.39 | −0.02 | −1.05 | −2.53 | −0.39 | −0.45 | −0.01 | −1.05 | −3.20 | −0.52 |
| GBCAL | 0.31 | 0.31 | 0.38 | 1.34 | 0.39 | 0.29 | 0.50 | 0.60 | 1.80 | 0.12 | 0.32 | 0.55 | 0.61 | 1.57 | 0.31 |
| GBELE | −0.14 | 0.04 | −0.54 | −1.91 | 0.00 | −0.10 | 0.48 | −0.45 | −0.73 | −0.27 | −0.13 | 0.54 | −0.44 | −1.63 | −0.21 |
| GBTOT | −0.55 | −1.45 | −3.07 | −3.34 | −3.61 | −0.67 | −1.48 | −3.41 | −2.58 | −4.01 | −0.79 | −1.46 | −3.41 | −3.42 | −3.91 |

**Fig. 5.** Binding mode of (A) Inhibitor-1, (B) Inhibitor-2, and (C) Inhibitor-3 in the allosteric site of PTP1B. The inhibitor is represented in stick format and the carbon atom is in cyan. The residues near the inhibitor binding pocket are shown as sticks and the carbon atom is in magenta. (For interpretation of the references to color in this figure legend, the reader is referred to the web version of this article.)
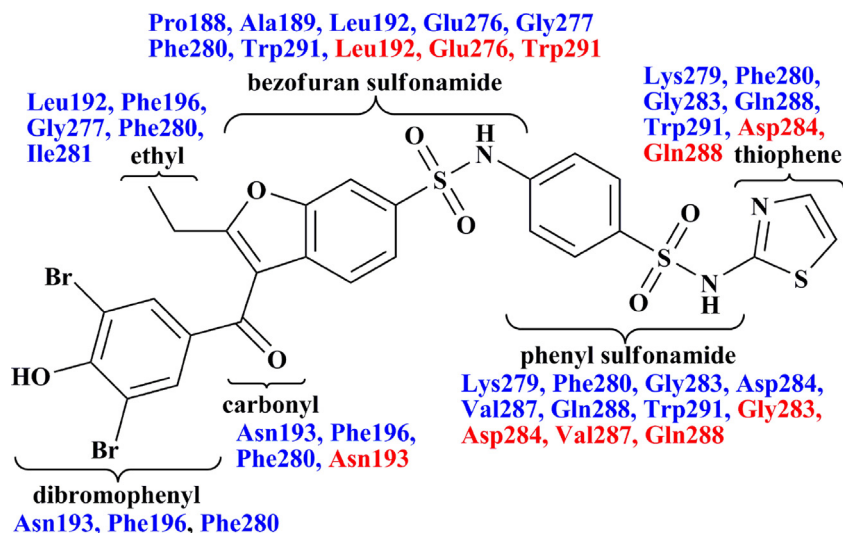


**Fig. 6.** Representation of substructures present in allosteric inhibitors and interacting residues. Inhibitor-3 structure with the residues that form interactions with few or all atoms of the sub-structures is shown. Blue colored residues make van der Waals interactions while red colored residues show electrostatic interactions. (For interpretation of the references to color in this figure legend, the reader is referred to the web version of this article.)

Additionally, the *B*-factor of this residue in complexes of Inhibitors-1, 2 and 3 was decreased sequentially (12.20, 11.01 and 8.51, respectively) (Supplementary information, Table S2). Thus, both interaction energy and stability followed the increasing trend of activity values of Inhibitors-1, 2 and 3. It can be concluded that the interactions with Pro188 could be one of the mechanisms through which inhibitors result in the allosteric inhibition. This also confirmed the findings of Cui et al., which suggested that improving the VDW interactions with this residue would enhance the allosteric inhibition capability of inhibitors [19].

H-bond between Asn193 side chain nitrogen atom and the carbonyl oxygen atom of inhibitors was observed in the X-ray structures of the three inhibitors (1T48, 1T49, 1T4J) (Fig. 5). We studied this bond during simulation and was found to be stable for Inhibitors-1 and 3 with the occupancy of 67.49% and 66.93% respectively (Fig. 7). For Inhibitor-2, it was consistent for an initial period of 11 ns with the occupancy of 31.39%. Afterwords it ceased showing the occupancy of only 6.72% for the remaining period. Termination of this bond just after the initiation of MD had also been observed in MD studies performed by Bharatham et al. [15] and Baskaran et al. [17]. This bond was also found to be essential, as the compounds lacking the carbonyl of sulfonyl groups have been reported to be devoid of any inhibitory activity [36]. However, even after the termination of H-bond, Asn193 maintained contact with inhibitor forming non-bonded interactions with carbonyl group and dibromo-phenyl ring (Table 3 and Fig. 6). Observations from the previous PTP1B MD studies showed that the Leu192 and Phe196 are part of the hydrophobic pocket

that accommodates benzofuran core of Inhibitor-2 [10,15]. We explored distance and binding energy between the Inhibitor-2 and these residues throughout the simulation to confirm these observations. The average minimum distance of Inhibitor-2 form Leu192 and Phe196 was observed to be 0.31 and 0.34 nm, confirming the stacking of the inhibitor at the hydrophobic allosteric pocket (Fig. 5, Supplementary information, Figs. S3 and S4). Other inhibitors also showed similar binding mode and molecular interactions because, for the Inhibitor-1, these distances were found to be 0.29 and 0.34 nm respectively, while for Inhibitor-3, they were found to be
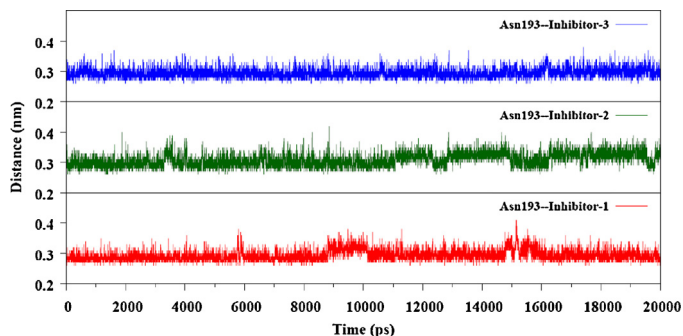


**Fig. 7.** Distance between side chain nitrogen atom of Asn193 and carbonyl oxygen of inhibitor-1 (red), Inhibitor-2 (green) and Inhibitor-3 (blue). (For interpretation of the references to color in this figure legend, the reader is referred to the web version of this article.)

0.29 and 0.35 nm, respectively (Supplementary information, Figs. S3 and S4). Leu192 provided GBVDW interactions energy of nearly −2.50 kcal/mol, while, Phe196, being more hydrophobic, provided nearly −3.70 kcal/mol of GBVDW energy toward the binding of each inhibitor (Table 3).

Interestingly our study observed a new residue, Ala189, as a part of this hydrophobic pocket, forming non-bonded interactions with the sulfonyl and benzofuran ring atoms, through side chain methyl group (Fig. 5). It remained in contact with Inhibitors-1, 2 and 3 throughout the simulation, at the average minimum distance of 0.35, 0.36, and 0.35 nm, respectively, stabilizing benzofuran core of the inhibitors (Supplementary information, Fig. S5). It provided GBTOT energy −1.5 kcal/mol toward the binding of each inhibitor (Table 3).

### 3.5.2. α6 helix residues

The α6 helix, comprising of residues Ala264-Ile279, is adjacent to the a7 helix and Phe280 of it is the prime residue that anchors the binding of allosteric inhibitor [10]. We explored the interactions of this residue along with other residues of the same helix with three inhibitors. Phe280 formed hydrophobic and π−π stacking interactions with the benzofuran core of three inhibitors. In addition, it interacted with all the sub-structures of three inhibitors throughout the production simulation (Fig. 6, and Supplementary information, Fig. S6), stabilizing the inhibitors at the allosteric site. It was noticed that, GBVDW energy contribution increased (−3.38 kcal/mol, −6.71 kcal/mol, −7.49 kcal/mol for Inhibitors-1, 2 and 3, respectively) with the number of sub-structures (Inhibitor-1 < Inhibitor-2 < Inhibitor-3) (Table 4). Phe280 also made unfavorable VDW interactions with the Inhibitor-3 (1.25 kcal/mol) which can be attributed its close contacts with the benzofuran, phenyl and thiazole rings of Inhibitor-3. As thiazole ring is absent, unfavorable interactions were not significant in the other inhibitors (0.45 kcal/mol and 0.60 kcal/mol for Inhibitor-1 and Inhibitor-2, respectively).

In addition to Phe280, Gly277 also favorably contributed to the binding of three inhibitors prominently through VDW interactions (Table 4, Supplementary information, Fig. S7). It mainly interacted with the ethyl side chain and benzofuran ring of the three inhibitors (Figs. 5 and 6) and contributed GBVDW energy of −0.73 kcal/mol for the binding of Inhibitor-1 and nearly −1 kcal/mol to the binding of Inhibitor-2 and Inhibitor-3 (Table 4). Another residue, Lys279, formed VDW interactions with the phenyl sulfonamide group of Inhbitors-2 and 3 through side chain carbon atoms, (Figs. 6 and 5, and Supplementary information, Fig. S8). It additionally interacted with the thiazole ring of Inhibitor-3. As it interacted with a fewer numbers of atoms in Inhibitor-2, it showed lesser GBVDW energy contribution (−1.51 kcal/mol) compared to the contribution (−1.80 kcal/mol) for Inhibitor-3. However, for Inhibitor-1, only −0.21 kcal/mol energy was contributed because of the absence of the phenyl ring (Tables 4 and 1). Ile281 showed variable contribution to the binding of inhibitors (−0.22 kcal/mol, −0.62 kcal/mol and −1.08 kcal/mol for Inhibitors-1, 2 and 3 respectively) (Table 4). The contribution was mainly through the VDW interactions with the ethyl group of the inhibitors.

We explored the interactions of Glu276 as crystal structures have shown a strong H-bond between the side chain carboxylate of Glu276 and benzofuran sulfonamide nitrogen atom of Inhibitor-2 and Inhibitor-3 (Fig. 5) [9]. Formation of this bond was thought to be one of the main reasons of greater than 40-fold increase in the affinity for Inhibitor-3, as compared to Inhibitor-1 against PTP1B. In the MD study by Bharatham et al., this H-bond was observed to be maintained throughout the simulation period in PTP1B-Inhibitor-2 complex [14]. Consistent with this finding, a stable bond was also observed for Inhibitor-2, as well as for Inhibitor-3, in this study (Figs. 5 and 8). Even though this interaction was translated in the

**Table 4**
Binding energy between residues of α6 helix and allosteric inhibitors in kcal/mol.

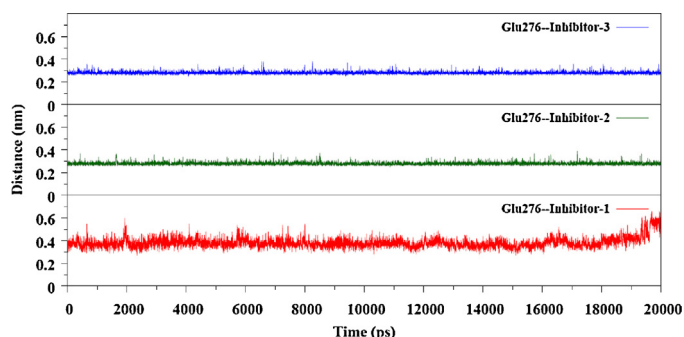| Residue | Inhibitor-1 | | | | | Inhibitor-2 | | | | | Inhibitor-3 | | | | |
|---|---|---|---|---|---|---|---|---|---|---|---|---|---|---|---|
| | Gly277 | Lys279 | Phe280 | Ile281 | Glu276 | Gly277 | Lys279 | Phe280 | Ile281 | Glu276 | Gly277 | Lys279 | Phe280 | Ile281 | Glu276 |
| VDW | −0.70 | −0.21 | −3.02 | −0.26 | −1.25 | −1.02 | −1.43 | −6.04 | −0.83 | −1.74 | −1.02 | −1.72 | −6.68 | −1.15 | −1.59 |
| GBSUR | −0.03 | 0.00 | −0.36 | −0.01 | −0.16 | −0.04 | −0.08 | −0.67 | −0.09 | −0.23 | −0.03 | −0.08 | −0.81 | −0.10 | −0.22 |
| GBVDW | −0.73 | −0.21 | −3.38 | −0.27 | −1.42 | −1.06 | −1.51 | −6.71 | −0.92 | −1.97 | −1.05 | −1.80 | −7.49 | −1.25 | −1.81 |
| ELE | −0.25 | −0.78 | −0.08 | 0.01 | 1.90 | −0.39 | 0.86 | −0.16 | 0.24 | −10.87 | −0.41 | 3.24 | −0.18 | 0.17 | −11.00 |
| GBCAL | 0.56 | 0.07 | 0.53 | 0.04 | 0.54 | 0.66 | −2.03 | 0.76 | 0.06 | 12.76 | 0.57 | −2.64 | 1.43 | 0.00 | 13.03 |
| GBELE | 0.31 | −0.71 | 0.45 | 0.05 | 2.44 | 0.27 | −1.17 | 0.60 | 0.30 | 1.89 | 0.16 | 0.60 | 1.25 | 0.17 | 2.03 |
| GBTOT | −0.42 | −0.92 | −2.93 | −0.22 | 1.03 | −0.79 | −2.68 | −6.11 | −0.62 | −0.08 | −0.89 | −1.20 | −6.24 | −1.08 | 0.22 |

**Fig. 8.** Distance between oxygen atom of Glu276 and benzofuran sulfonamide nitrogen atom of inhibitor-1 (red), Inhibitor-2 (green) and Inhibitor-3 (blue). (For interpretation of the references to color in this figure legend, the reader is referred to the web version of this article.)

ELE energy contribution of $-10.87$ kcal/mol and $-11.00$ kcal/mol to the binding of Inhibitor-2 and Inhibitor-3 respectively, it was negated by the higher solvation energies, i.e. 12.76 kcal/mol and 13.03 kcal/mol respectively (Table 4). This bond could not be formed for Inhibitor-1 as the participating hydrogen is substituted with a methyl group.

### 3.5.3. α6–α7 loop residues

Out of the five residues that comprise the α6–α7 loop, two residues favorably contributed to the binding of Inhibitor-2, four residues contributed to the binding of Inhibitor-3, while no residue favored with GBTOT energy greater than $-0.50$ kcal/mol to the binding of Inhibitor-1 (Table 5). It suggested that the α6–α7 loop provides differential affinities to the Inhibitors-1, 2 and 3. We critically analyzed energy contribution by individual residue of this loop. It was noticed that, the residue Gly283 provides higher potency to the Inhibitor-2 and Inhibitor-3 as compared to Inhibitor-1. It remained at an average minimum distance of 0.36 nm from both the inhibitors and interacted with the sulfonyl atoms of the phenyl sulfonamide group. Additionally, it interacted with the thiazole ring of Inhibitor-3, contributing a little higher GBVDW energy to Inhibitor-3 over Inhibitor-2 ($-0.79$ kcal/mol and $-0.61$ kcal/mol respectively). Inhibitor-1 being small and lacking in phenyl sulfonyl group remained farther from the residue (average minimum distance of 0.91 nm, Supplementary information, Fig. S9) and hence could not obtain favorable binding contribution from the residue. Furthermore, backbone nitrogen atom (donor) of it formed H-bond with phenyl sulfonamide nitrogen atom of Inhibitor-2 and with thiazole ring nitrogen atom of Inhibitor-3. Latter being more consistent interaction contributed higher toward the binding of Inhibitor-3 than Inhibitor-2 (GBELE $-0.39$ kcal/mol and $-0.78$ kcal/mol, respectively) (Table 5).

Similar to Gly283, Asp284 also provided differential energy contribution to the binding of three inhibitors. Asp284 was observed to be involved in stable non-bonded interactions with the phenyl sulfonamide group of inhibitors 2 and 3, as well as with thiazole ring of Inhibitor-3. (Fig. 5 and Supplementary information, Fig. S10). Accordingly, it showed a GBVDW energy of $-0.74$ kcal/mol and $-1.09$ kcal/mol for Inhibitor-2 and Inhibitor-3 respectively (Table 5). Greater contribution for Inhibitor-3 was seen because of the interactions with thiazole ring.

In case of electrostatic interactions, Asp284 formed three H-bonds as follows:

1. H-bond between the backbone nitrogen atom (donor) of Asp284 and phenyl sulfonyl oxygen atom (acceptor) of Inhibitor-2.

2. H-bond between the backbone oxygen atom (acceptor) of Asp284 and phenyl sulfonyl nitrogen atom (donor) of Inhibitor-3.

3. H-bond between the backbone nitrogen atom (donor) of Asp284 and thiazole nitrogen (acceptor) atom of Inhibitor-3.

The H-bond analysis showed 28.64% occupancy for the first H-bond for Inhibitor-2. This bond was not formed in Inhibitor-3 complex, as the presence of thiazole ring increased the distance between the two atoms. Interestingly, the second H-bond was observed for the Inhibitor-3 only. The absence of second H-bond in Inhibitor-2 complex was scrutinized and it was noticed that the formation of the first bond reorients the backbone carbonyl oxygen in opposite direction so as to maintain the trans character of the peptide bond. It moved the bonding backbone oxygen away from the phenyl sulfonyl nitrogen of Inhibitor-2 hence, forbidding the formation of H-bond. For Inhibitor-3, it was a stable bond showing the occupancy of 93.28%. The third H-bond was also observed only for Inhibitor-3, as thiazole ring is absent in the Inhibitor-2 but showed the occupancy of only 3.30%. Because of the presence of these two H-bonds in Inhibitor-3, GBTOT energy offered by Asp284 was found to be greater ($-1.39$ kcal/mol) as compared to Inhibitor-2 ($-0.51$ kcal/mol) (Table 5). It resulted in providing greater affinity to the Inhibitor-3. None of the above H-bonds were possible for the Inhibitor-1, as it lacked substructures (phenyl sulfonamide and thiazole) taking part in these bonds. The consecutive serine residues 285 and 286 formed hydrophobic interactions only with the Inhibitor-3 (Supplementary information, Figs. S11 and S12). Both collectively contributed $-2.00$ kcal/mol of binding energy providing higher affinity over the other two inhibitors (Table 5).

### 3.5.4. α7 helix residues

Structural and MD studies have elucidated the importance of α7 helix in the allosteric inhibition of PTP1B. Residues Gln288, Ser295, and Glu297 of this helix formed H-bond network with the residues of α3 helix and β9–β10 loop [12]. It was observed to be an essential requirement for the closure of WPD-loop. Allosteric inhibitor has been reported to terminate these interactions by placing itself between the helices α3–α6–α7. It is believed that the allosteric inhibitor occupies the site of Trp291 by the displacement, stabilizing itself between the hydrophobic groove formed by the residues Trp291, Phe280, Phe196 and Leu192 [10,15]. Trp291 was reported to be fundamental to this pocket hence, we studied its interactions. Even though displaced from its position Trp291 maintained its contact with the inhibitors throughout the simulation, at an average minimum distance of 0.33, 0.33 and 0.34 nm (Supplementary information, Fig. S13), making a contribution of $-3.62$ kcal/mol, $-2.81$ kcal/mol, and $-2.27$ kcal/mol to the binding of Inhibitors-1, 2 and 3 respectively (Table 6). It interacted with the benzofuran ring, confirming its role in the formation of hydrophobic pocket and stabilization of inhibitors (Fig. 5). Besides this, it also formed another novel binding pocket along with the residues Phe280, Val287 and Gln288, accommodating phenyl sulfonamide group of Inhibitors-2 and 3 and the thiazole group of Inhibitor-3 (Fig. 9). In case of Inhibitor-1, this pocket was not well formed because of the absence of the above groups.

Val287, a α7 helix residue, showed hydrophobic interactions with three inhibitors throughout simulation (Supplementary information, Fig. S14). It interacted with the dimethyl amino group of Inhibitor-1, phenyl sulfonamide ring of Inhibitors-2 and 3, while additional thiazole group of Inhibitor-3 (Fig. 5). It provided an equal GBVDW energy contribution to the Inhibitor-1 and Inhibitor-2 ($\sim -1.50$ kcal/mol), but greater contribution to Inhibitor-3 ($-1.95$ kcal/mol) (Table 6) because of the additional thiazole group. In addition to VDW interactions, it also formed

**Table 5**
Binding energy between residues of α6–α7 loop and Inhibitors-1, 2 and 3 in kcal/mol.

| Residue | Inhibitor-2 | | | Inhibitor-3 | | |
|---|---|---|---|---|---|---|
| | Gly283 | Asp284 | Gly283 | Asp284 | Ser285 | Ser286 |
| VDW | −0.56 | −0.73 | −0.69 | −1.01 | −0.57 | −0.76 |
| GBSUR | −0.05 | −0.01 | −0.10 | −0.08 | 0.00 | −0.01 |
| GBVDW | −0.61 | −0.74 | −0.79 | −1.09 | −0.57 | −0.77 |
| ELE | −0.34 | −1.14 | −0.50 | −3.42 | −0.13 | −0.13 |
| GBCAL | −0.05 | 1.37 | −0.28 | 3.12 | −0.06 | −0.11 |
| GBELE | −0.39 | 0.23 | −0.78 | −0.30 | −0.19 | −0.24 |
| GBTOT | −1.00 | −0.51 | −1.57 | −1.39 | −0.76 | −1.01 |

electrostatic interactions through the formation of H-bond with the phenyl sulfonamide oxygen atom of Inhibitor-3. For other two inhibitors, this H-bond was not observed and thus, provided greater affinity to the Inhibitor-3. This H-bond also helped Val287 to remain in contact with Inhibitor-3, providing consistent non-bonded interactions. Glu288, another α7 helix residue, was involved in the formation of second hydrophobic pocket and it showed consistent interactions with Inhibitor-2 and Inhibitor-3 (Fig. 9 and Supplementary information, Fig. S15). Gln288 being the next residue of Val287, its distance from the dimethyl nitrogen atom increased further and it did not show any non-bonded interactions with Inhibitor-1. In case of Inhibitor-2, it stabilized the phenyl sulfonamide group, while in case of Inhibitor-3. It steadied interactions with phenyl sulfonamide and thiazole ring. Additional interactions with thiazole ring brought greater GBVDW energy contributions for Inhibitor-3 (Table 6) and thus a greater affinity over Inhibitor-2. Glu288 also formed two H-bonds with the Inhibitor-3. First H-bond was formed between the side chain nitrogen atom (donor) and thiazole ring nitrogen (acceptor) and had the occupancy of 23.32%. The second H-bond was between the backbone nitrogen (donor) and thiazole ring nitrogen (acceptor). This H-bond formed with the occupancy of only 2%, but can be seen as supportive for the first H-bond. Both interactions collectively provided GBELE contribution of −1.54 kcal/mol toward the binding of Inhibitor-3. These H-bonds provided greater affinity to Inhibitor-3 over the other two inhibitors.

*3.5.5. Energy contribution from helices and loop*

We calculated total contributions made by α3, α6, α7 helix and α6–α7 loop in the binding of Inhibitors-1, 2 and 3 by summing up the GBTOT energy of each residue present in these secondary structure elements (Table 7). It was observed that the helices α3 and α6 play a substantial role in the stabilization of inhibitors while α3 helix, α6 helix and α6–α7 loop provide differential affinity to the three inhibitors. Binding to the α3 and α6 helices was predominantly driven by the hydrophobic interactions. Even though residue

Asn193 of α3 helix and Glu276 of α6 helix were involved in continuous H-bond interactions, electrostatic interactions played a minor role in the molecular recognition of inhibitors (Table 7). It suggested that these helices prefer binding with the hydrophobic substructures of ligands. Among these helices, α3 helix equally contributed to the binding of three inhibitors (nearly −14 kcal/mol), while α6 helix showed equal contributions to Inhibitor-2 and Inhibitor-3 (nearly −11.00 kcal/mol), and reduced contribution to the small size molecule Inhibitor-1 (−4.89 kcal/mol). Total energy contribution by α6–α7 loop increased with the size of inhibitor (0.02, −1.69 and −4.86 kcal/mol for Inhibitors-1, 2 and 3). Hydrophobic (GBVDW) and electrostatic (GBELE) energy components also followed the same trend (Table 7), providing differential affinity to the inhibitors. Similar to α3 and α6 helices, binding to α7 helices was also driven by non-polar interactions. It can be perceived that the three residues of α7 helix (Val287, Gln288 and Phe291) were involved in the formation of the hydrophobic pocket accommodating phenyl and thiazole ring of Inhibitors-2 and 3. It also provided greater affinity to Inhibitor-3, over Inhibitors-1 and 2, through both electrostatic and hydrophobic interactions.

## 4. Drug design aspects

The affinity of the three inhibitors (Inhibitor-1 < Inhibitor-2 < Inhibitor-3) is influenced by hydrophobic interactions which in turn are related to the number of rings (2, 3 and 4 respectively). Out of the 17 residues that show considerable binding, nine, fifteen and seventeen residues have provide greater than −0.50 kcal/mol hydrophobic contributions to the binding of Inhibitors-1, 2 and 3 respectively. This suggested the importance of hydrophobic groups in the inhibitors. Affinity of the present inhibitors can be increased by the replacement of aromatic rings with more hydrophobic groups. Similarly, the ethyl group of inhibitors replaced with more bulky groups can improve the activity of inhibitors. The side chains of nine residues (Pro188, Asn193, Lys279, Glu276, Asp284, Ser285, Ser286, Trp291 and Gln288) were observed to be involved
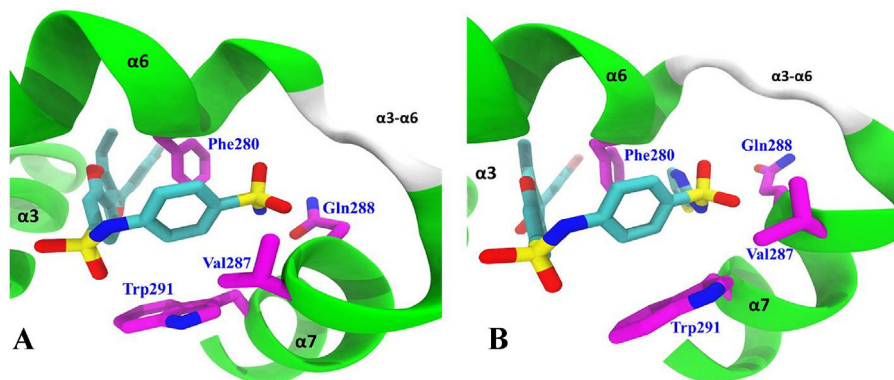


**Fig. 9.** Conformation of (A) Inhibitor-2 and (B) Inhibitor-3 in the allosteric site of PTP1B. loop α6–α7, and helices α3, α6, α7 are shown. Hydrophobic pocket formed by the residues Phe280, Val287, Gln288 and Trp291 accommodates phenyl sulfonamide group of Inhibitors-2 and 3 and thiazole group of Inhbiitor-3.

**Table 6**
Binding energy between residues of α7 helix and Inhibitor-1, 2 and 3 in kcal/mol.

| Residue | Inhibitor-1 | | Inhibitor-2 | | | Inhibitor-3 | | |
|---|---|---|---|---|---|---|---|---|
| | Val287 | Trp291 | Val287 | Trp291 | Gln288 | Val287 | Trp291 | Gln288 |
| VDW | −1.36 | −4.22 | −1.40 | −3.13 | −1.04 | −1.78 | −2.89 | −1.81 |
| GBSUR | −0.12 | −0.41 | −0.13 | −0.35 | −0.09 | −0.17 | −0.29 | −0.17 |
| GBVDW | −1.48 | −4.63 | −1.53 | −3.48 | −1.13 | −1.95 | −3.18 | −1.98 |
| ELE | −0.83 | −0.30 | 0.27 | −1.90 | −0.21 | −1.53 | −1.58 | −2.04 |
| GBCAL | 1.00 | 1.31 | −0.42 | 2.57 | 0.10 | 0.53 | 2.49 | 0.50 |
| GBELE | 0.17 | 1.01 | −0.15 | 0.67 | −0.11 | −1.00 | 0.91 | −1.54 |
| GBTOT | −1.31 | −3.62 | −1.68 | −2.81 | −1.24 | −2.95 | −2.27 | −3.52 |

**Table 7**
Binding energy contribution by secondary structure elements, calculated by summing energy contribution of individual element residues, toward the binding of three allosteric inhibitors.

| | α-helix | | | α6-helix | | | α6-α7 loop | | | α7 helix | | |
|---|---|---|---|---|---|---|---|---|---|---|---|---|
| | Inhibitor-1 | Inhibitor-2 | Inhibitor-3 | Inhibitor-1 | Inhibitor-2 | Inhibitor-3 | Inhibitor-1 | Inhibitor-2 | Inhibitor-3 | Inhibitor-1 | Inhibitor-2 | Inhibitor-3 |
| VDW | −11.11 | −12.64 | −13.19 | −5.80 | −11.73 | −12.84 | −0.24 | −1.59 | −3.20 | −8.59 | −5.94 | −6.92 |
| GBSUR | −1.14 | −1.18 | −1.16 | −0.57 | −1.10 | −1.26 | 0.00 | −0.06 | −0.19 | −0.82 | −0.58 | −0.63 |
| GBVDW | −12.25 | −13.82 | −14.35 | −6.37 | −12.83 | −14.10 | −0.24 | −1.65 | −3.39 | −9.41 | −6.52 | −7.55 |
| ELE | −4.61 | −3.37 | −5.46 | 0.42 | −11.62 | −9.45 | −0.97 | −0.94 | −4.08 | −1.31 | −1.69 | −4.63 |
| GBCAL | 2.96 | 3.41 | 4.93 | 1.05 | 12.73 | 12.89 | 1.23 | 0.89 | 2.62 | 4.07 | 2.31 | 3.19 |
| GBELE | −1.65 | 0.04 | −0.53 | 1.47 | 1.11 | 3.44 | 0.26 | −0.05 | −1.46 | 2.76 | 0.62 | −1.44 |
| GBTOT | −13.90 | −13.78 | −14.88 | −4.90 | −11.71 | −10.66 | 0.02 | −1.70 | −4.85 | −6.65 | −5.90 | −8.99 |

in H-bonding or salt bridge interactions with the electronegative atoms/groups of inhibitors. This provides an opportunity to substitute the rings with heterocyclic rings which may improve the VDW interactions while maintaining the hydrophobic interactions. Residues Phe280, Val287, and Gln290 of PTP1B are replaced with Cys278, Ile285, and Arg288 in TCPTP. These residues have made the major energy contribution in binding of PTP1B inhibitors. Residue Phe280 formed hydrophobic interactions with almost all sub-structures of the inhibitors and contributed the highest VDW energy to the binding of inhibitors. It is replaced with the small and less hydrophobic Cys278 in TCPTP, and hence, improving the interactions with Phe280 will improve the selectivity of PTP1B inhibitors against TCPTP. Residue Val287 is replaced with Ile285, a residue of similar hydrophobicity. Residue Ile285 can decrease the binding of inhibitors to TCPTP due to steric hindrance, made by additional methyl group. Positively charged residue Arg288 replaces neutral residue Gln290 of PTP1B. Substitution of the positively charged group can be used to impart unfavorable binding with Arg288 and thus, the selectivity over TCPTP.

## 5. Conclusion

α7 helix of PTP1B was modeled separately using the open state PTP1B template in presence of allosteric Inhibitors-1, 2 and 3. Three models were then subjected to MD simulations. All the complexes were stable during the simulation and inhibitors showed consistent interactions with several residues of the allosteric site. Residues Gly283, Asp284, Ser285, Ser286, Val287, Gln288 and Trp291 of the modeled loop and helix were found to be critical in binding and providing differential affinity to the allosteric inhibitors. Modeled elements also led to the identification of a novel, induced hydrophobic pocket formed by the residues Val287, Gln288, Trp291 and Phe280. Among the secondary structures that surround the allosteric site viz. α3, α6, α7 helices and α6–α7 loop, each provided favorable hydrophobic interactions to three inhibitors. α6 helix provided greater affinity to Inhibitors-2 and 3 over Inhibitor-1, while α6–α7 loop and α7 helix provided greater affinity to Inhibitor-3 over Inhibitors-1 and 2. Conformations sampled during MD were found to follow the geometrical descriptor values of the open conformation. It confirmed the findings of Wiesmann et al., which concluded that the allosteric inhibitors prevent the formation of active form of the enzyme by blocking mobility of the WPD-loop [10]. High $B$-factors of α7 helix residues in PTP1B complexes led to the speculation that the higher flexibility of residues was responsible for the disordered or absence of α7 helix in the co-crystal structures of allosteric inhibitors. Energetic analyses of complexes revealed that the inhibitor binding was driven by the VDW interactions. Residue Phe280 can be considered as the anchor of these interactions as it interacted with almost all atoms of the inhibitors. This residue can provide good selectivity as it is replaced with the serine in TCPTP. This study provides useful insights for the rational design of more potent and selective allosteric inhibitors of PTP1B.

## Acknowledgments

## Appendix A. Supplementary data

Supplementary data associated with this article can be found, in the online version, at http://dx.doi.org/10.1016/j.jmgm.2013.08.001.

## References

[1] K.A. Kenner, E. Anyanwu, J.M. Olefsky, J. Kusari, Protein-tyrosine phosphatase 1B is a negative regulator of insulin- and insulin-like growth factor-I-stimulated signaling, J. Biol. Chem. 271 (1996) 19810–19816.
[2] K.K. Bence, M. Delibegovic, B. Xue, C.Z. Gorgun, G.S. Hotamisligil, B.G. Neel, B.B. Kahn, Neuronal PTP1B regulates body weight, adiposity and leptin action, Nat. Med. 12 (2006) 917–924.
[3] M. Elchebly, P. Payette, E. Michaliszyn, W. Cromlish, S. Collins, A.L. Loy, D. Normandin, A. Cheng, J. Himms-Hagen, C.C. Chan, C. Ramachandran, M.J. Gresser, M.L. Tremblay, B.P. Kennedy, Increased insulin sensitivity and obesity resistance in mice lacking the protein tyrosine phosphatase-1B gene, Science 283 (1999) 1544–1548.
[4] S. Koren, I.G. Fantus, Inhibition of the protein tyrosine phosphatase PTP1B: potential therapy for obesity, insulin resistance and type-2 diabetes mellitus, Best Pract. Res. Clin. Endocrinol. Metab. 21 (2007) 621–640.
[5] H.M. Berman, J. Westbrook, Z. Feng, G. Gilliland, T.N. Bhat, H. Weissig, I.N. Shindyalov, P.E. Bourne, The protein data bank, Nucleic Acids Res. 28 (2000) 235–242.
[6] S. Lee, Q. Wang, Recent development of small molecular specific inhibitor of protein tyrosine phosphatase 1B, Med. Res. Rev. 27 (2007) 553–573.
[7] J.N. Andersen, O.H. Mortensen, G.H. Peters, P.G. Drake, L.F. Iversen, O.H. Olsen, P.G. Jansen, H.S. Andersen, N.K. Tonks, N.P.H. Moller, Structural and evolutionary relationships among protein tyrosine phosphatase domains, Mol. Cell. Biol. 21 (2001) 7117–7136.
[8] L.F. Iversen, K.B. Moller, A.K. Pedersen, G.H. Peters, A.S. Petersen, H.S. Andersen, S. Branner, S.B. Mortensen, N.P. Moller, Structure determination of T cell protein-tyrosine phosphatase, J. Biol. Chem. 277 (2002) 19982–19990.
[9] K.E. You-Ten, E.S. Muise, A. Itie, E. Michaliszyn, J. Wagner, S. Jothy, W.S. Lapp, M.L. Tremblay, Impaired bone marrow microenvironment and immune function in T cell protein tyrosine phosphatase-deficient mice, J. Exp. Med. 186 (1997) 683–693.
[10] C. Wiesmann, K.J. Barr, J. Kung, J. Zhu, D.A. Erlanson, W. Shen, B.J. Fahr, M. Zhong, L. Taylor, M. Randal, Allosteric inhibition of protein tyrosine phosphatase 1B, Nat. Struct. Mol. Biol. 11 (2004) 730–737.
[11] Z. Jia, D. Barford, A.J. Flint, N.K. Tonks, Structural basis for phosphotyrosine peptide recognition by protein tyrosine phosphatase 1B, Science 268 (1995) 1754–1758.
[12] J. Montalibet, K. Skorey, D. McKay, G. Scapin, E. Asante-Appiah, B.P. Kennedy, Residues distant from the active site influence protein-tyrosine phosphatase 1B inhibitor binding, J. Biol. Chem. 281 (2006) 5258–5266.
[13] S.C. Kamerlin, R. Rucker, S. Boresch, A targeted molecular dynamics study of WPD loop movement in PTP1B, Biochem. Biophys. Res. Commun. 345 (2006) 1161–1166.
[14] S.C. Kamerlin, R. Rucker, S. Boresch, A molecular dynamics study of WPD-loop flexibility in PTP1B, Biochem. Biophys. Res. Commun. 356 (2007) 1011–1016.
[15] K. Bharatham, N. Bharatham, Y.J. Kwon, K.W. Lee, Molecular dynamics simulation study of PTP1B with allosteric inhibitor and its application in receptor based pharmacophore modeling, J. Comput. Aided Mol. Des. 22 (2008) 925–933.
[16] E.O. Olmez, B. Alakent, Alpha7 helix plays an important role in the conformational stability of PTP1B, J. Biomol. Struct. Dyn. 28 (2011) 675–693.
[17] S.K. Baskaran, N. Goswami, S. Selvaraj, V.S. Muthusamy, B.S. Lakshmi, Molecular dynamics approach to probe the allosteric inhibition of PTP1B by chlorogenic and cichoric acid, J. Chem. Inf. Model. 52 (2012) 2004–2012.
[18] J.Y. Lee, K.W. Jung, E.R. Woo, Y. Kim, Docking study of biflavonoids, allosteric inhibitors of protein tyrosine phosphatase 1B, Bull. Korean Chem. Soc. 29 (2008) 1479–1484.
[19] W. Cui, Y.H. Cheng, L.L. Geng, D.S. Liang, T.J. Hou, M.J. Ji, Unraveling the allosteric inhibition mechanism of PTP1B by free energy calculation based on umbrella sampling, J. Chem. Inf. Model. 53 (2013) 1157–1167.
[20] R. Kumar, R.N. Shinde, D. Ajay, M.E. Sobhia, Probing interaction requirements in PTP1B inhibitors: a comparative molecular dynamics study, J. Chem. Inf. Model. 50 (2010) 1147–1158.
[21] R.N. Shinde, M. Elizabeth Sobhia, Geometrical criteria for characterizing open and closed states of WPD-loop in PTP1B, J. Mol. Struct. 1017 (2012) 79–83.
[22] A.K. Pedersen, G.G. Peters, K.B. Moller, L.F. Iversen, J.S. Kastrup, Water-molecule network and active-site flexibility of apo protein tyrosine phosphatase 1B, Acta Crystallogr. D: Biol. Crystallogr. 60 (2004) 1527–1534.
[23] N. Eswar, B. Webb, M.A. Marti-Renom, M.S. Madhusudhan, D. Eramian, M. Shen, U. Pieper, A. Sali, Comparative protein structure modeling using Modeller, Curr. Protoc. Protein Sci. (2007) 2.9.1–2.9.31.
[24] J. Wang, R.M. Wolf, J.W. Caldwell, P.A. Kollman, D.A. Case, Development and testing of a general amber force field, J. Comput. Chem. 25 (2004) 1157–1174.
[25] A. Jakalian, B.L. Bush, D.B. Jack, C.I. Bayly, Fast efficient generation of high quality atomic charges. AM1 BCC model: I. Method, J. Comput. Chem. 21 (2000) 132–146.
[26] D.A. Pearlman, D.A. Case, J.W. Caldwell, W.S. Ross, T.E. Cheatham, S. DeBolt, D. Ferguson, G. Seibel, P. Kollman, AMBER a package of computer programs for applying molecular mechanics, normal mode analysis, molecular dynamics and free energy calculations to simulate the structural and energetic properties of molecules, Comput. Phys. Commun. 91 (1995) 1–41.
[27] W.L. Jorgensen, J. Chandrasekhar, J.D. Madura, R.W. Impey, M.L. Klein, Comparison of simple potential functions for simulating liquid water, J. Chem. Phys. 79 (1983) 926–935.

[28] D.A. Case, T.E. Cheatham, T.H. Darden 3rd, R. Gohlke, K.M. Luo, A. Merz Jr., C. Onufriev, B. Simmerling, R.J. Wang, Woods, The Amber biomolecular simulation programs, J. Comput. Chem. 26 (2005) 1668–1688.
[29] W.F. van Gunsteren, H.J.C. Berendsen, Algorithms for macromolecular dynamics and constraint dynamics, Mol. Phys. 34 (1977) 1311–1327.
[30] T. Darden, D. York, L. Pedersen, Particle mesh Ewald: an $N.\log(N)$ method for Ewald sums in large systems, J. Chem. Phys. 98 (1993), 10089-10089.
[31] T.E. Cheatham 3rd, J. Srinivasan, D.A. Case, P.A. Kollman, Molecular dynamics and continuum solvent studies of the stability of polyG–polyC and polyA–polyT DNA duplexes in solution, J. Biomol. Struct. Dyn. 16 (1998) 265–280.
[32] B. Kuhn, P.A. Kollman, Binding of a diverse set of ligands to avidin and streptavidin: an accurate quantitative prediction of their relative affinities by a combination of molecular mechanics and continuum solvent models, J. Med. Chem. 43 (2000) 3786–3791.
[33] B. Honig, A. Nicholls, Classical electrostatics in biology and chemistry, Science 268 (1995) 1144–1149.
[34] A. Onufriev, D. Bashford, D.A. Case, Exploring protein native states and large-scale conformational changes with a modified generalized born model, Proteins: Struct. Funct., Bioinf. 55 (2004) 383–394.
[35] H. Gohlke, C. Kiel, D.A. Case, Insights into protein–protein binding by binding free energy calculation and free energy decomposition for the Ras–Raf and Ras–RalGDS complexes, J. Mol. Biol. 330 (2003) 891–913.
[36] Y.B. Tang, D. Lu, Z. Chen, C. Hu, Y. Yang, J.Y. Tian, F. Ye, L. Wu, Z.Y. Zhang, Z. Xiao, Design, synthesis and insulin-sensitising effects of novel PTP1B inhibitors, Bioorg. Med. Chem. Lett. 23 (2013) 2313–2318.